Effect of the central atom potential on the extended fine structure above appearance potential thresholds

G. E. Laramore

Department of Radiation Oncology, University of Washington Hospital, Seattle, Washington 98195

T. L. Einstein, L. D. Roelofs, and Robert L. Park

Department of Physics and Astronomy, University of Maryland, College Park, Maryland 20742
(Received 5 September 1979)

The formalism previously given for describing the extended fine structure above appearance-potential-spectroscopy (APS) thresholds is extended by incorporating the effects of the excited "central" atom potential in an exact manner. The excitation-matrix elements are expressed in terms of the exact wave functions of the central atom potential. This introduces a "phase renormalization" into the excitation-matrix elements and eliminates a previously noted "phase difference" between single- and multiple-scattering calculations employing a plane-wave basis set. A series of approximations is then made which leads to an expression for the APS extended fine structure in terms of sinusoidal functions and hence provides a rationale for a Fourier-transform analysis. Simple model calculations assuming a constant "bare" excitation-matrix element, a spherically symmetric electronic density of states, and only S-wave scattering from the atomic cores are performed for a cluster of atoms having the atomic geometry of bulk vanadium. These calculations display the major predictions of the formalism and indicate that for a given system there may be some optimal energy range for data analysis. The problem of electron characteristic losses is considered, and it is pointed out that in the small-momentum-transfer limit the simple dipole selection rules appropriate to a photon-excitation process again apply. This may obviate many of the problems introduced by multiple angular momentum final states in the APS process.

I. INTRODUCTION

During the past year, it has been noted that final-state scattering phenomena can produce extended fine structure above electron-excited atomic-absorption thresholds in solids,[1,2] and a general formalism[3] has been put forth which qualitatively describes the observed features. Experimentally one monitors either the total yield of soft x rays or the total sample current as a function of the energy of an incident electron beam. Changes are brought out by differentiating with respect to the incident beam energy, and it is in the derivative mode that both the main excitation peaks and their attendant extended fine structure are observed. The derivative procedure has the effect of "pinning" one of the excited final state electrons at the Fermi energy, and the resulting approximate expression is very similar[4] to that obtained for the extended x-ray-absorption fine structure (EXAFS). It was then postulated[2,4] that the APS extended fine structure could be approximately described by a set of sinusoidally varying functions as in EXAFS.[5,6] This meant that the appearance-potential-spectroscopy (APS) extended fine structure could be analyzed by simple Fourier-transform techniques and simple model calculations,[4] and actual data analysis[2,7] tended to bear this out. The current interplay between theory and experiment has pointed out

some deficiencies in the original theoretical treatment, and this paper extends the original formulation in an attempt to remedy some of these difficulties.

The initial calculations were formulated in terms of a plane-wave basis set and this led to an overall "phase shift" between extended fine structure calculated in the single- and multiple-scattering limits.[3,4] While this phase shift did not affect the Fourier-transform procedure, its origin was puzzling since it did not seem to occur in analogous EXAFS calculations.[8] Here we reformulate the problem of calculating the APS extended fine structure by taking into account the renormalization effects of multiple scattering from the potential of the excited central atom. This leads to a new set of basis functions which are the exact solutions of the Schrödinger equation in the central-atom potential. We show that there are two main effects of this renormalization: (1) The "bare" excitation-matrix elements are defined in terms of the partial-wave components of the true central-atom wave functions instead of in terms of spherical Bessel functions arising from a partial wave expansion of plane waves. This provides justification for ongoing work in which the excitation-matrix elements are being evaluated in the orthogonalized-plane-wave (OPW) approximation and also via the $X\alpha$ scattered-wave molecular-orbital method. (2) Treat-

2108

ing the scattering from the central atom exactly results in the same phase for the geometrically induced oscillations, regardless of whether the scattering from the *remaining* atoms is treated in the single- or multiple-scattering limits. We then make a small atom approximation in which the radius of curvature of the incident wave front is neglected and show that in the single-scattering limit this leads to an EXAFS-like result in which the extended fine structure can be approximately described in terms of a set of sinusoidally varying functions. Explicit expressions for the phase factors entering these functions are given. The results are formally more complex than initially postulated,[2,4] and it is shown that in polycrystalline materials analogous terms also arise from the scattering of the incident electron prior to the excitation of the atomic core level. Near threshold, final-state scattering effects dominate, and it is shown that restricting the data range used in the Fourier-transform procedure allows one to better separate the desired signal from spurious peaks arising from initial-state scattering processes. This helps to remove an ambiguity in previous work on the Fourier-transform method of analysis.[4] The excitation-matrix element in APS is the Coulomb interaction and so,

unlike EXAFS there are in principle a large number of partial wave components which contribute to the final result. However, in practice only a small number of components are important—particularly for K-level excitations. Moreover, if we restrict ourselves to the limit of small momentum transfer during the excitation process, then we return to the dipole selection rules of EXAFS. Such a situation may be realizable in characteristic loss measurements in a high-energy electron microscope.

In the next section we describe the theoretical formalism and show the modifications introduced by the renormalized wave functions. We also derive an EXAFS-like expression for the APS extended fine structure by taking the appropriate limits. In Sec. III we demonstrate the main predictions of the formalism through simple model calculations assuming only S-wave scattering from the atomic core, a spherically symmetric one-electron density of states, and a constant bare excitation-matrix element. In Sec. IV we discuss the small-momentum-transfer limit of a characteristic loss process and point out that this returns us to the familiar dipole selection rules. Finally, in Sec. V we summarize our results.

II. FORMALISM

Our starting point is the expression given in Ref. 3 for the total transition rate for an incident electron exciting a core-level electron of a given atom in a solid:

$$\langle \dot{\Phi}_I \rangle_s = \frac{2\pi}{\hbar} N_c \sum_{\vec{k}_f, \vec{k}_{f'} > P_F} \delta(E_i - E_f - E_{f'} - \Delta)[\tfrac{3}{4}|M^c_{\uparrow\uparrow}(\vec{k}_i; \vec{k}_f, \vec{k}_{f'})|^2 + \tfrac{1}{4}|M^c_{\uparrow\downarrow}(\vec{k}_i; \vec{k}_f, \vec{k}_{f'})|^2] . \tag{2.1}$$

In Eq. (2.1) $\langle\ \rangle_s$ indicates an average over the spin of the incident electron, N_c is the number of electrons in the atomic shell under consideration (assumed to be closed), $E_i(\vec{k}_i)$ is the energy (momentum) of the incident electron, $E_f(\vec{k}_f)$ and $E_{f'}(\vec{k}_{f'})$ are the energies (momenta) of the two excited final-state electrons, Δ is the binding energy of the core electron (we will ultimately define this relative to the zero of energy in a muffin-tin approximation), and $M^c_{\uparrow\uparrow}$ and $M^c_{\uparrow\downarrow}$ are the respective matrix elements for the two final state electrons emerging in a triplet or singlet spin state. In the appearance potential spectroscopies, one does not energy resolve the excited final-state electrons and so sees a sum over all possible final states with momenta greater than the Fermi momentum P_F. The matrix elements for the excitation process are given by

$$M^c_{\uparrow\uparrow,\uparrow\downarrow}(\vec{k}_i; \vec{k}_f, \vec{k}_{f'}) = \int d^3r_1 d^3r_2 \langle \psi_{\vec{k}_f}, \psi_{\vec{k}_{f'}} | \vec{r}_2, \vec{r}_1 \rangle_{(\mp)} \frac{e^2}{|\vec{r}_1 - \vec{r}_2|} \langle \vec{r}_1, \vec{r}_2 | \psi_{\vec{k}_i}, \phi_c \rangle_{(\mp)} , \tag{2.2}$$

where

$$\langle \vec{r}_1, \vec{r}_2 | \psi_{\vec{k}_i} \phi_c \rangle_{(\mp)} = 2^{-1/2}[\psi_{\vec{k}_i}(\vec{r}_1)\phi_c(\vec{r}_2) \mp \psi_{\vec{k}_i}(\vec{r}_2)\phi_c(\vec{r}_1)] \tag{2.3a}$$

and

$$\langle \vec{r}_1, \vec{r}_2 | \psi_{\vec{k}_f}, \psi_{\vec{k}_{f'}} \rangle_{(\mp)} = 2^{-1/2}[\psi_{\vec{k}_f}(\vec{r}_1)\psi_{\vec{k}_{f'}}(\vec{r}_2) \mp \psi_{\vec{k}_f}(\vec{r}_2)\psi_{\vec{k}_{f'}}(\vec{r}_1)] \tag{2.3b}$$

are appropriately antisymmetrized (symmetrized) spatial components of one-electron low-energy-electron-diffraction (LEED)-like wave functions $\psi_{\vec{k}}(\vec{r})$ and core electron wave functions $\phi_c(\vec{r})$. We work in terms of the partial wave-components of the matrix elements defined through

$$M^c_{\uparrow\uparrow,\uparrow\uparrow}(\vec{k}_i;\vec{k}_f,\vec{k}_{f'}) = \sum_{LL_1L_2} M^{cL}_{\uparrow\uparrow,\uparrow\uparrow L_1 L_2}(k_i;k_f,k_{f'})Y_L(\Omega_i)Y^*_{L_1}(\Omega_f)Y^*_{L_2}(\Omega_{f'}),$$

(2.4)

where $Y_L = Y_{lm}$ are the usual spherical-harmonic functions and

$$\sum_L \equiv \sum_{l=0}^{\infty}\sum_{m=-l}^{l} .$$

(2.5)

This allows us to perform the angular portion of the final-state summation in Eq. (2.1) immediately. We further assume that our sample has only short-range order and so we effectively see an average over the direction of the incident beam. Equation (2.1) hence becomes

$$\langle \dot{\mathcal{P}}_I \rangle_s = \frac{N_c}{2\hbar}\int_\mu^\infty dE_f\, dE_{f'}\,\delta(E_i - \Delta - E_f - E_{f'})\rho(E_f)\rho(E_{f'})\sum_{LL_1L_2}[\tfrac{3}{4}|M^{cL}_{\uparrow\uparrow,L_1L_2}(k_i;k_f,k_{f'})|^2$$

$$+\tfrac{1}{4}|M^{cL}_{\uparrow\uparrow,L_1L_2}(k_i;k_f,k_{f'})|^2],$$

(2.6)

where μ is the Fermi energy.

Our problem thus reduces to the calculation of the one-electron LEED-like wave functions in the field of the excited central atom. In coordinate space this is given by[9]

$$\psi_{\vec{k}}(\vec{r}) = \chi_{\vec{k}}(\vec{r}) + \int d^3r_1\, d^3r_2\, G_0(\vec{r} - \vec{r}_1)$$

$$\times T(\vec{r}_1,\vec{r}_2)\chi_{\vec{k}}(\vec{r}_2),$$

(2.7)

where

$$\chi_{\vec{k}}(\vec{r}) = (2\pi)^{-3/2}\exp(i\vec{k}\cdot\vec{r}),$$

(2.8a)

and

$$G_0(\vec{r} - \vec{r}_1) = \frac{\int d^3k_1}{(2\pi)^3}\frac{\exp[i\vec{k}_1\cdot(\vec{r} - \vec{r}_1)]}{E - \left(\dfrac{\hbar^2k_1^2}{2m}\right) - \sum(E)}$$

(2.8b)

is the Green's function describing the propagation of the electron between successive scatterings with the atomic cores. The effect of inelastic-collision processes with the conduction electrons is taken into account via a complex self-energy

$$\sum(E) = \frac{-i\hbar^2}{m\lambda_{ee}}\left(\frac{2m}{\hbar^2}E\right)^{1/2},$$

(2.9)

where E is the energy of the electron defined *relative* to the muffin-tin zero, which we take to be V_0 below the vacuum level. Strictly speaking, λ_{ee} is energy dependent and becomes quite long as E approaches the Fermi energy. Hence, near the Fermi energy it might be better to use wave functions obtained from energy-band calculations instead of LEED-like wave functions. $T(\vec{r}_1,\vec{r}_2)$ is the coordinate-space representation of the T matrix which can be written in terms of the individual t matrices from the atomic sites. Separating out explicitly the scattering from the central-atom potential, the T matrix is given symbolically by

$$T = t_0 + T' + t_0G_0T' + T'G_0t_0 + t_0G_0T'G_0t_0,$$

(2.10)

where t_0 is the single-site t matrix describing the scattering from the central-atom potential (taken to be site 0) and T' is the T matrix describing the sum of all possible scattering events where the initial and final scattering events do not take place at the central atom. The first, third, and fifth terms on the right-hand side of Eq. (2.10) were not included in the analysis of Ref. 3. In evaluating Eq. (2.10) we can use different potentials for the initial- and the final-state scattering in order to allow for the changed potential of the excited central atom. Substituting Eq. (2.10) into Eq. (2.7), we obtain

$$\psi_{\vec{k}}(\vec{r}) = \phi_{\vec{k}}(\vec{r}) + \int d^3r_1\, d^3r_2\, G_c(\vec{r},\vec{r}_1)$$

$$\times \sum_{nn'\neq 0}T'_{nn'}(\vec{r}_1,\vec{r}_2)\phi_{\vec{k}}(\vec{r}_2),$$

(2.11)

where

$$\phi_{\vec{k}}(\vec{r}) = \chi_{\vec{k}}(\vec{r}) + \int d^3r_1\, d^3r_2\, G_0(\vec{r} - \vec{r}_1)$$

$$\times t_0(\vec{r}_1,\vec{r}_2)\chi_{\vec{k}}(\vec{r}_2)$$

(2.12)

is the exact wave function for the electron propagating in the central-atom potential, $G_c(\vec{r},\vec{r}_1)$ is the renormalized central atom Green's function given by

$$G_c(\vec{r},\vec{r}_1) = \frac{\sum_{\vec{k}}\phi_{\vec{k}}(\vec{r})\phi^*_{\vec{k}}(\vec{r}_1)}{E - (\hbar^2k^2/2m) - \sum(E)},$$

(2.13)

and

$$T'_{nn'}(\vec{r}_1,\vec{r}_2) = \delta_{nn'}t_n(\vec{r}_1,\vec{r}_2)$$

$$+ \sum_{n_1\neq n}\int d^3r_3\, d^3r_4\, t_n(\vec{r}_1,\vec{r}_3)$$

$$\times G_0(\vec{r}_3 - \vec{r}_4)T'_{n_1n'}(\vec{r}_4,\vec{r}_2)$$

(2.14)

is the usual T matrix used in LEED work.[10] Note that the intermediate site summation index, n_1

can include the central atom. $\phi_{\vec{k}}(\vec{r})$ is discussed in the Appendix, where it is noted that, apart from an overall phase factor, its partial-wave components correspond to the usual muffin-tin wave functions obtained by numerically integrating the Schrödinger equation inside the muffin-tin radius and matching to phase-shifted plane-wave components at the muffin-tin radius. Specifically,

$$\phi_{\vec{k}}(\vec{r}) = \frac{1}{(2\pi)^{3/2}} \sum_L \phi_k^L(r) Y_L^*(\Omega_r) Y_L(\Omega_k), \qquad (2.15)$$

where inside the central-atom muffin tin

$$\phi_k^L(r < R_{mt}) = \overline{\phi}_k^{-L}(r) \exp(i\delta_l), \qquad (2.16)$$

and outside the central-atom muffin tin

$$\phi_k^L(r > R_{mt}) = 2\pi(i)^l \exp(i\delta_l)$$
$$\times [\exp(i\delta_l) h_l^{(1)}(kr)$$
$$+ \exp(-i\delta_l) h_l^{(2)}(kr)]. \qquad (2.17)$$

In Eqs. (2.16) and (2.17) $\overline{\phi}_r^{-L}(r)$ is the numerical solution to the radial Schrödinger equation inside the central-atom muffin tin as defined in the Appendix, $h_l^{(1,2)}$ are spherical Hankel functions of the first and second type, and δ_l is the lth partial-wave phase shift for the central atom which would be calculated using different potentials for the initial and final states.

We next write

$$T'_{nn'}(\vec{r}_1, \vec{r}_2) = \frac{\int d^3k_1 d^3k_2}{(2\pi)^6} T'_{nn'}(\vec{k}_1, \vec{k}_2) \exp[i\vec{k}_1 \cdot (\vec{r}_1 - \vec{R}_n) - i\vec{k}_2 \cdot (\vec{r}_2 - \vec{R}_{n'})], \qquad (2.18)$$

where $\vec{R}_n$ denotes the position of the nth atomic site and make a partial-wave expansion of $T'_{nn'}(\vec{k}_1, \vec{k}_2)$

$$T'_{nn'}(\vec{k}_1, \vec{k}_2) = \sum_{L_1 L_2} T'^{L_1 L_2}_{nn'}(k_1, k_2) Y_{L_1}^*(\Omega_{k_1}) Y_{L_2}(\Omega_{k_2}). \qquad (2.19)$$

Making the usual partial-wave expansion of the exponential functions (cf. A6) and substituting Eqs. (2.13), (2.15), (2.18), and (2.19) into Eq. (2.11) we obtain

$$\psi_{\vec{k}}(\vec{r}) = \sum_{LL'} \frac{\psi_{kL}^{L'}(r)}{(2\pi)^{3/2}} Y_{L'}^*(\Omega_r) Y_L(\Omega_k), \qquad (2.20a)$$

where

$$\psi_{kL}^{L'}(r) = \phi_k^L(r) \delta_{LL'} + \sum_{L_1 L_2 L_3 L_4 L_5} \frac{\int d^3r_1 d^3r_2 d^3k_1 d^3k_2 d^3k_3}{(2\pi)^9} \sum_{nn' \neq 0} \left(\frac{\phi_{k_1}^{L'}(r) Y_{L'}(\Omega_{k_1})}{E - (\hbar^2 k_1^2/2m) - \sum(E)} \phi_{k_1}^{*L_1}(r_1) Y_{L_1}(\Omega_{r_1}) Y_{L_1}^*(\Omega_{k_1}) \right)$$
$$\times [(4\pi)^2 (i)^{l_4 - l_5} j_{l_4}(k_2|\vec{r}_1 - \vec{R}_n|) Y_{L_4}^*(\Omega_{\vec{r}_1} - \vec{R}_n) Y_{L_4}(\Omega_{k_2})$$
$$\times T'^{L_2 L_3}_{nn'}(k_2, k_3) Y_{L_2}^*(\Omega_{k_2}) Y_{L_3}(\Omega_{k_3}) j_{l_5}(k_3|\vec{r}_2 - \vec{R}_{n'}|)$$
$$\times Y_{L_5}(\Omega_{\vec{r}_2} - \vec{R}_{n'}) Y_{L_5}^*(\Omega_{k_3})][\phi_k^L(r_2) Y_L^*(\Omega_{r_2})], \qquad (2.20b)$$

where the terms in Eq. (2.20b) have been grouped as to their function of origin. Following Lee and Pendry,[8] we note that we need r inside the central-atom muffin tin in order to evaluate the necessary excitation-matrix elements. The other coordinate vectors in Eq. (2.20b) describe the propagation of the electron from the lattice site $n' \neq 0$, through intermediate lattice sites to site $n \neq 0$. Hence, we can take $\vec{r}_1$ and $\vec{r}_2$ as lying outside the central-atom muffin-tin radius and expand the relevant wave functions, respectively, about $\vec{R}_n$ and $\vec{R}_{n'}$. Specifically, we need to expand $\phi_{k_1}^{*L_1}(r_1)$ about $\vec{R}_n$ in the limit where $|\vec{r}_1 - \vec{R}_n| < R_n$ and keeping only the portion of the wave function which is incoming to the site 0, we obtain

$$\phi_{k_1}^{*L_1}(r_1) Y_{L_1}(\Omega_{r_1}) = 2\pi(-i)^{l_1} [h_{l_1}^{*(2)}(k_1 r_1) = h_{l_1}^{(1)}(k_1 r_1)] Y_{L_1}(\Omega_{r_1})$$
$$= 2\pi(-i)^{l_1} \sum_{\overline{L}_1 \overline{L}_2} (4\pi)(i)^{l_1 + \overline{l}_1 - \overline{l}_2} I(\overline{L}_2; \overline{L}_1, L_1) h_{l_1}^{(1)}(k_1 R_n)$$
$$\times Y_{\overline{L}_2}(\Omega_{\vec{r}_1} - \vec{R}_n) Y_{\overline{L}_1}^*(\Omega_{R_n}) j_{\overline{l}_2}(k_1|\vec{r}_1 - \vec{R}_n|), \qquad (2.21)$$

where

$$I(\overline{L}_2; \overline{L}_1, L_1) = \int (d\Omega) Y_{\overline{L}_2}^*(\Omega) Y_{\overline{L}_1}(\Omega) Y_{L_1}(\Omega). \qquad (2.22)$$

Similarly we expand $\phi_k^{L_6}(r_2)$ about $\vec{R}_{n'}$ in the limit where $|\vec{r}_2 - \vec{R}_{n'}| < R_{n'}$ and, keeping only the portion of the

wave function outgoing at the site 0, we obtain

$$\phi_k^{L_6}(r_2)Y_{L_6}^*(\Omega_{r_2}) = 2\pi(i)^{l_6}\exp(2i\delta_{l_6})\sum_{L_1L_2}(4\pi)(-i)^{l_6+\bar{l}_1-\bar{l}_2}I(\bar{L}_2;\bar{L}_1,L_6)$$

$$\times h_{l_1}^{(1)}(kRn')Y_{L_2}^*(\Omega_{\vec{r}_2}-\vec{R}_{n'})Y_{\bar{L}}(\Omega_{R_{n'}})j_{\bar{l}_2}(k|\vec{r}_2-\vec{R}_{n'}|) \,. \tag{2.23}$$

Substituting Eqs. (2.21) and (2.23) into Eq. (2.20), the integrations over $d^3r_1\,d^2r_2\,d^3k_2\,d^3k_3\,(d\Omega_{k_1})$ can be directly performed and the integral over $dk_1\,k_1^2$ performed using contour techniques.[3] We obtain for $r < R_{mt}$

$$\psi_{kL}^{L'}(r) = \exp(i\delta_l)\bar{\phi}_k^{L}(r)\delta_{LL'} + \exp(i\delta_l)\bar{\phi}_K^{L'}(r)A_{L'L}(K,k)\,, \tag{2.24}$$

where

$$A_{L'L}(K,k) = \exp(i\delta_l + i\delta_{l'})\sum_{L_1L_2}\sum_{nn'\neq 0}\frac{-2\pi^2 i\hbar^2}{mk}\tilde{G}_{0n}^{L'L_1}(K)T_{nn'}^{L_1L_2}(K,k)G_{n'0}^{L_2L}(k)\,. \tag{2.25}$$

In Eq. (2.25)

$$K \equiv K(E) = \left\{\frac{2m}{\hbar^2}\left[E - \sum(E)\right]\right\}^{1/2} \tag{2.26}$$

is a wave vector defined on the complex energy shell, and

$$\tilde{G}_{0n}^{L'L_1}(K) = \sum_{L_3}\frac{(i)^{l_3}}{2\pi}\frac{mK}{\hbar^2}I(L';L_3,L_1)h_{l_3}^{(1)}(KR_n)Y_{L_3}^*(\Omega_{R_n}) \tag{2.27a}$$

and

$$G_{n'0}^{L_2L}(k) = \sum_{L_3}\frac{(-i)^{l_3}}{2\pi}\frac{mk}{\hbar^2}I(L_2;L_3,L)h_{l_3}^{(1)}(kR_{n'})Y_{L_3}(\Omega_{R_{n'}}) \tag{2.27b}$$

are structural Green's functions similar to those used in LEED calculations. The resulting excitation-matrix elements are given by

$$M_{\cdots,L_1L_2}^{cL}(k_i;k_f,k_{f'}) = \sqrt{2}\,\exp(i\delta_l - i\delta'_{l_1} - i\delta'_{l_2})$$

$$\times\left(\bar{W}_{\cdots,L_1L_2}^{cL}(k_i;k_f,k_{f'}) + \sum_L \bar{W}_{\cdots,L_1L_2}^{cL}(K(E_i);k_f,k_{f'})A_{\bar{L}L}^-(K(E_i),k_i) + \cdots\right.$$

$$+ \sum_{L\bar{L}_1}\bar{W}_{\cdots,\bar{L}L_2}^{c\bar{L}}(K(E_i);K(E_f),k_{f'})A_{\bar{L}L}^-(K(E_i),k_i)A_{\bar{L}_1L_1}^*(K(E_f),k_f) + \cdots$$

$$+ \sum_{L\bar{L}_1\bar{L}_2}\bar{W}_{\cdots,\bar{L}_1\bar{L}_2}^{c\bar{L}}(K(E_i);K(E_f),K(E_{f'}))A_{\bar{L}L}^-(K(E_i),k_i)$$

$$\left.\times A_{\bar{L}_1L_1}^*(K(E_f),k_f)A_{\bar{L}_2L_2}^*(K(E_{f'}),k_{f'})\right)\,, \tag{2.28}$$

where representative terms of each type have been explicitly shown. The unprimed phase shifts are evaluated for the unexcited-central-atom initial-state potential, and the primed phase shifts are to be evaluated for the excited-central-atom final-state potential. As before,[3] we will ultimately restrict ourselves to scattering events on the complex energy shell, i.e., $k \to K(E)$, in evaluating the $A_{L'L}$. The new "bare" excitation wave functions $\bar{W}$ are given by

$$\bar{W}_{\cdots,L_1L_2}^{cL}(k_i;k_f,k_{f'}) = \frac{16e^2}{\sqrt{2\pi}}\sum_L\int dr_1 dr_2\,\frac{r_1^2 r_2^2}{2\bar{l}+1}\frac{r_<^{\bar{l}}}{r_>^{\bar{l}+1}}\times\bar{\phi}_{k_i}^{L}(r_1)R_{n_c l_c}(r_2)$$

$$\times[I(L;\bar{L},L_1)I(\bar{L};L_2,L_c)\bar{\phi}_{k_f}^{*L_1}(r_1)\bar{\phi}_{k_{f'}}^{*L_2}(r_2)$$

$$\mp I(L;\bar{L},L_2)I(\bar{L};L_1,L_c)\bar{\phi}_{k_f}^{*L_1}(r_2)\bar{\phi}_{k_{f'}}^{*L_2}(r_1)]\,, \tag{2.29}$$

and are similar to the bare excitation-matrix elements of Ref. 3 except that the partial-wave components of the exact, unbound, central-atom wave functions have replaced spherical Bessel functions arising from a partial-wave expansion of a plane-wave basis set. In Eq. (2.29) $r_<(r_>)$ is the lesser (greater) of r_1 and r_2 and $R_{n_c l_c}(r_2)$ is the radial component of the core-level wave function. Work is in progress[7,12] evaluating Eq. (2.29) using an OPW approximation for the $\overline{\phi}_k^L(r)$, and it appears that only a relatively modest number of matrix elements make the dominant contributions. Equation (2.28) is an exact expression within the context of the defined model potential and can be readily evaluated using existing LEED programs to calculate $T'_{nn'}(K(E), K(E))$. To derive the analog of the EXAFS expression[5,6] for the APS extended fine structure, we follow Lee and Pendry[8] and make a series of approximations in evaluating the $A_{L'L}$. As a first step we return to Eq. (2.20b) and initially perform the integral over

$(d\Omega_{k_1})$ to obtain $\delta_{L_1 L_1}$. Then we make plane-wave expansions of $\phi_{k_1}^{*L 1}(r_1)$ about $\vec{R}_n$ and of $\phi_k^{L 6}(r_2)$ about $\vec{R}_{n'}$ making sure that the wave functions have the correct values at the relevant expansion sites. This is essentially a "small-atom" approximation in that the curvature of the wave front is neglected as it impinges on the scattering site. Specifically, using Eq. (2.17),

$$\phi_{k_1}^{*L 1}(r_1) Y_{L_1}(\Omega_{r_1}) = (2\pi)(-i)^{l_1} h_{l_1}^{(1)}(k_1 R_n) Y_{L_1}(\Omega_{R_n})$$
$$\times \exp[-i\vec{k}_1 \cdot (\vec{r}_1 - \vec{R}_n)], \qquad (2.30)$$

where $\vec{k}_1 = -k_1 \hat{R}_n$, and

$$\phi_k^{L 6}(r_2) Y_{L_6}^*(\Omega_{r_2}) = (2\pi)(i)^{l_6}$$
$$\times \exp(2i\delta_{l_6}) h_{l_6}^{(1)}(k R_{n'}) Y_{L_6}^*(\Omega_{R_{n'}})$$
$$\times \exp[i\vec{k} \cdot (\vec{r}_2 - \vec{R}_{n'})], \qquad (2.31)$$

where $\vec{k} = k\hat{R}_{n'}$. The plane waves are then expanded in the usual way, and we obtain an expression analogous to Eq. (2.24) with

$$A_{L'L}(K, k) = \exp(i\delta_l + i\delta_{l'}) \sum_{L_1 L_2} \sum_{nn' \neq 0} (-2\pi^2 i\hbar^2/mk)[(mk/2\pi\hbar^2)(-i)^{l'+1} h_{l'}^{(1)}(K R_n) Y_{L'}(\Omega_{R_n}) Y_{L_1}^*(\Omega_{-R_n})]$$

$$\times T_{nn'}^{'L_1 L_2}(K, k)[(mk/2\pi\hbar^2)(i)^{l+1} h_l(k R_{n'}) Y_L^*(\Omega_{R_{n'}}) Y_{L_2}(\Omega_{R_{n'}})]. \qquad (2.32)$$

In Eq. (2.32) terms have been grouped to show their correspondence with terms in Eq. (2.25). This is a simplification over Eq. (2.25) in that we no longer have to do the intermediate partial-wave sums necessary to define the structural Green's functions.

The next level of approximation is to restrict ourselves to the single scattering limit, i.e.,

$$T_{nn'}^{'L_1 L_2}(K, k) \to t_n^{L_1}(K, k)\delta_{L_1 L_2}\delta_{nn'}, \qquad (2.33)$$

where on the complex energy shell[13]

$$t_n^{L_1}(K, K) = (4\pi\hbar^2 i/mK)[\exp(2i\delta_l^n) - 1]. \qquad (2.34)$$

This allows us to perform the sum over L_1 and L_2 in closed form since

$$\sum_{L_1} t_n^{L_1}(K, K) Y_{L_1}^*(\Omega_{-R_n}) Y_{L_1}(\Omega_{R_n}) = f_n(K, \pi), \qquad (2.35)$$

where $f_n(K, \pi)$ is the total back-scattering amplitude for the nth site corresponding to momentum K. This gives

$$A_{L'L}(K, K) \simeq \exp(i\delta_l + i\delta_{l'}) \sum_{n \neq 0} (i)^{l-l'-1} (mK/\hbar^2) h_{l'}^{(1)}(K R_n) f_n(K, \pi) h_l^{(1)}(K R_n) Y_{L'}(\Omega_{R_n}) Y_L^*(\Omega_{R_n}). \qquad (2.36)$$

Passing to the asymptotic limit

$$h_l^{(1)}(K R_n) \to (-i)^{l+1} \exp(iK R_n)/K R_n \qquad (2.37)$$

and breaking the sum over n into a sum over the identical atoms in a given shell, j, followed by a sum over shells, Eq. (2.36) can be written as

$$A_{L'L}(K, K) \simeq \sum_j \frac{mi}{\hbar^2} \frac{\exp[2iK R_j + il'\pi + \psi_j(K) + \alpha(j; L'L) + \delta_l + \delta_{l'}]}{K R_j^2} \times |f_j(K, \pi)| |S_j(L', L)|, \qquad (2.38)$$

where

$$f_j(K, \pi) = |f_j(K, \pi)| \exp[i\psi_j(K)] \tag{2.39}$$

and

$$S_j(L', L) = \sum_n Y_{L'}(\Omega_{R_n}) Y_L^*(\Omega_{R_n}) = |S_j(L', L)| \exp[i\alpha(j; L', L)] \tag{2.40}$$

(where n is in the jth shell) is a type of structure factor for the jth shell.

In Ref. 4 it was shown that the dominant contribution to the energy derivative of the transition rate occurred when one of the final-state electrons went into a state at the Fermi energy and hence

$$\frac{d}{dE_i} \langle \dot{\mathcal{P}}_l \rangle_S \simeq \frac{N_c}{2\hbar} \rho(E_i + V_0 - \mu - \Delta)\rho(\mu)\Theta(E_i + V_0 - 2\mu - \Delta) \sum_{LL_1L_2} [\tfrac{3}{4} |M^{cL}_{\uparrow\uparrow,L_1L_2}(k_i; \bar{k}_f, P_F)|^2$$

$$+ \tfrac{1}{4} |M^{cL}_{\uparrow\uparrow,L_1L_2}(k_i; \bar{k}_f, P_F)|^2], \tag{2.41}$$

where

$$\bar{k}_f = [(2m/\hbar^2)(E_i + V_0 - \mu - \Delta)]^{1/2} \equiv [(2m/\hbar^2)\bar{E}_f]^{1/2} \tag{2.42}$$

and Θ is the Heaviside step function. For comparison with experiment we express E_i relative to the vacuum level, not the muffin-tin zero, and hence have explicitly added V_0 to it in Eqs. (2.41) and (2.42). Our final step is to subtract off the background term which involves only the direct excitation of the core level without any preceding or following scattering of the electrons from the neighboring atom and to evaluate Eq. (2.41) to *first order* in the scattering from the neighboring atoms using the asymptotic expression for $A_{L'L}$ given by Eq. (2.38). Letting G be the geometrical enhancement factor we obtain for the *oscillatory component*

$$\frac{d}{dE_i} G \simeq -\frac{N_c}{2\hbar} \rho(E_i + V - \mu - \Delta)\rho(\mu)\Theta(E_i + V_0 - 2\mu - \Delta)$$

$$\times \sum_{jLL_1L_2} \left[\tfrac{3}{4}\bar{W}^{cL}_{\uparrow\uparrow,L_1L_2}(k_i; \bar{k}_f, P_F) \right.$$

$$\times \left(\sum_L \bar{W}^{c\bar{L}}_{\uparrow\uparrow,L_1L_2}(k_i; \bar{k}_f, P_F) F^{\bar{L}L}_j(k_i; R_j) + \sum_{L_1} \bar{W}^{cL}_{\uparrow\uparrow,\bar{L}_1L_2}(k_i; \bar{k}_f, P_F) F^{\bar{L}_1L_1}_j(\bar{k}_f, R_j) \right)$$

$$+ \tfrac{1}{4}\bar{W}^{cL}_{\uparrow\uparrow,L_1L_2}(k_i; \bar{k}_f, P_F)$$

$$\times \left. \left(\sum_{L_1} \bar{W}^{c\bar{L}}_{\uparrow\uparrow,L_1L_2}(k_i; \bar{k}_f, P_F) F^{\bar{L}L}_j(k_i; R_j) + \sum_{L_1} \bar{W}^{cL}_{\uparrow\uparrow,\bar{L}_1,L_2}(k_i; \bar{k}_f, P_F) F^{\bar{L}_1L_1}_j(\bar{k}_f, R_j) \right) \right], \tag{2.43}$$

where

$$F^{L'L}_j(k, R_j) \equiv (m/\hbar^2) \sin[2kR_j + \psi_j(k) + \delta_{l'}(k) + \delta_l(k) + l'\pi + \alpha(j; L', L)] |f_j(k, \pi)| |S_j(L', L)|. \tag{2.44}$$

In Eq. (2.43) the central-atom phase shifts $\delta_l(k_i)$ are evaluated using the initial-state potential and the $\delta_l(\bar{k}_f)$ are evaluated using the final-state potential. Equation (2.43) has the same general form as that postulated in Ref. 4 but is more complex in that there is an additional internal summation over partial-wave components and there is also a contribution from the initial-state scattering. For realistic model potentials, in the large-k limit,[10] $|f_j(k, \pi)| \sim 1/k^2$, and so the ratio of final-state scattering to initial-state scattering scales like $(E_i/E_f)^{3/2}$. Hence we expect that transformation based upon only final-state scattering[4] should work best near threshold and the relative importance of initial-state scattering to become more important at large incident electron energies. In Sec. III we will demonstrate

that proper choice of the transform interval can greatly reduce spurious peaks in the transformed spectra. The extra partial-wave summation is more of a problem in that if many partial-wave components are important in evaluating the $\bar{W}^{cL}_{\uparrow\uparrow,\uparrow\uparrow,L_1L_2}$, the resulting expression gives rise to a very broad transformed spectrum since the "phase" of each of the summed sine functions is different. Nevertheless, it has proven possible to Fourier-transform the APS extended fine structure from transition metals and obtain the known nearest-neighbor shell spacings.[2,7,14]

III. MODEL CALCULATIONS

In this section we demonstrate the major predictions of the formalism through simple model

calculations performed in the spirit of the iso-
tropic-scatterer, inelastic-collision model of
early LEED work.[11] We will assume only S-wave
scattering from the atomic cores with the elec-
tron—single-atom elastic-scattering amplitude
being given by

$$t_n^{00}(K(E),K(E)) = \frac{4\pi\hbar^2 i}{mK(E)}[\exp(2_i\delta^n) - 1], \qquad (3.1)$$

where the δ^n are arbitrarily specified scattering
phase shifts and also assume constant bare exci-
tation-matrix elements

$$\overline{W}_{\uparrow\uparrow,\iota\iota}^c = \overline{W}_{\uparrow\uparrow,\iota\iota,00}^{c0}(4\pi)^{-3/2} = \text{const} \qquad (3.2)$$

and spherically symmetric one-electron densities
of states. This facilitates comparison with ear-
lier model calculations[3,4] using a plane-wave
basis set. Our model system will be a nine-atom
cluster consisting of a central atom and eight
nearest neighbors on a body-centered-cubic
lattice having the geometry of bulk vanadium.
This system was chosen because of current ex-
perimental[1,2,14] and theoretical[12] interest on vanad-
ium. We take $E_c = \Delta + V_0 = 591$ eV, which corre-
sponds to exciting the $2S$ level as determined from
a muffin-tin potential constructed from overlap-
ping atomic charge densities. These were calcu-
lated using the nonrelativistic limit of a Hartree-
Fock-Slater statistical-exchange approximation to
the Dirac equation.[15] This is a lower core-level
binding energy than the value $E_c = 628$ eV obtained
from electron-spectroscopy-for-chemical-analy-
sis (ESCA) measurements.[16] The value for the
Fermi energy relative to the muffin-tin zero of
$\mu = 12.5$ eV was estimated from the position of the
$l = 2$ partial-wave resonance as previously de-
scribed.[17] We emphasize that these are merely
representative numbers which are adequate for
our highly simplified model calculations which
may bear little correspondence to the experi-
mental situation where the $2p$ excitation domin-
ates.

We will use the same model potential for both
the initial- and final-state scattering and set the
scattering phase shifts equal to $\pi/2$, which maxi-
mizes the scattering cross sections within the
constraint of a unitary S-wave model potential.

Previous model calculations using a plane-wave
basis set[3,4] exhibited an overall phase shift be-
tween spectra calculated in the single- and
multiple-scattering limits. In Fig. 1 we compare
model calculations performed using a plane-wave
basis set with analogous calculations using Eqs.
(2.25) and (2.28). The single scattering limit is
taken using the complete spherical wave expan-

sion of Eq. (2.25). Part (a) shows curves calcu-
lated using the plane-wave basis set. Note the
overall phase difference between the curves
calculated in the single- and multiple-scattering
limits. There is an overall sign change which
has turned maximum into minimum. There are
some other differences between the curves in the
range 620–660 eV and also above 850 eV but the
main effect of multiple scattering is the overall
phase difference. This does not occur in the
curves of part (b), which were calculated using
the renormalized basis set. The phase of the
oscillations corresponds to the multiple-scatter-
ing curve of part (a). We can understand this
difference in terms of the renormalization effects
of the central-atom potential which is treated
numerically in the plane-wave calculations. This
occurs for the multiple-scattering calculations
but not for the single-scattering limit. Referring
to Eqs. (2.43) and (2.44), since the relevant
central-atom phase shifts are $\delta_0 = \delta_0' = \pi/2$, this
renormalization has the effect of changing the
oscillatory component from

$$\sin(\phi) \rightarrow \sin(\phi + \pi) = -\sin(\phi), \qquad (3.3)$$

and this accounts for the observed phase change.
We also note that there are some minor differ-
ences between the two curves of part (b) when one
goes from the single- to the multiple-scattering
limits, but as in EXAFS[8] it now appears that
single-scattering calculations may provide a
reasonable starting point for estimating the effects
of energy-dependent matrix elements and partial-
wave phase shifts.

In Fig. 2 we compare the full multiple-scatter-
ing calculation with the approximate expression
given by Eq. (2.43). The approximate expression
provides a good description of the frequency of the
oscillations out to $E_i \sim 720$ eV although the rela-
tive amplitudes of the oscillations are not well
described. We also note that the intial phase of
the oscillations is the same. Since the frequency
of the oscillation is sufficient to determine the
shell radii R_j if the momentum dependence of the
other phase contributions is known, this provides
some justification for a Fourier-transform method
of data analysis. However, unlike EXAFS it may
prove more difficult to obtain the shell coordina-
tion numbers, which are determined through the
amplitude of the oscillations.

Referring to Eq. (2.43) we see that final-state
scattering should dominate the oscillations near
threshold, while initial state scattering should
become more important far from threshold where
$E_i/\overline{E}_f \rightarrow 1$. To get some estimate of the energy
range where final-state scattering dominates we
return to the exact expression given by Eqs. (2.25)

VANADIUM

$V_0 = 18 eV, \lambda_{ee} = 8 \text{\AA}, \delta = \pi/2, \mu = 12.5 eV, E_c = 591 eV$

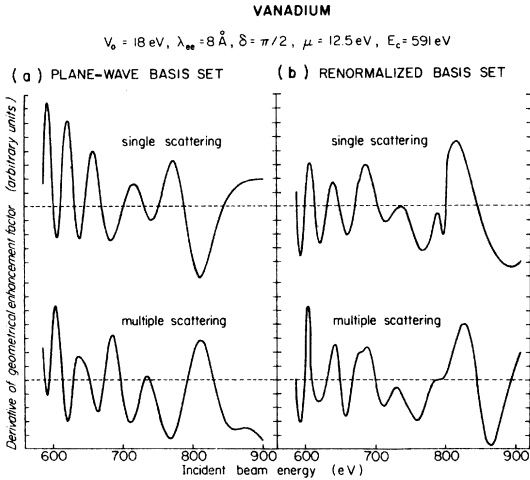(a) PLANE-WAVE BASIS SET   (b) RENORMALIZED BASIS SET

FIG. 1. Derivatives of the geometrical enhancement factor as a function of the incident beam energy. The calculations are for a cluster consisting of a central atom and its eight nearest neighbors with the geometry of bulk vanadium. Part (a) shows curves calculated using a plane-wave basis set as in Refs. 3 and 4, while part (b) shows curves calculated using the renormalized basis set of this work. Both the single- and multiple-scattering limits are shown. The other parameters used in the calculations are shown in the figure.

VANADIUM

$V_0 = 18 \text{ eV}, \lambda_{ee} = 8 \text{ \AA}, \delta = \pi/2, \mu = 12.5 \text{ eV}, E_c = 591 \text{ eV}$
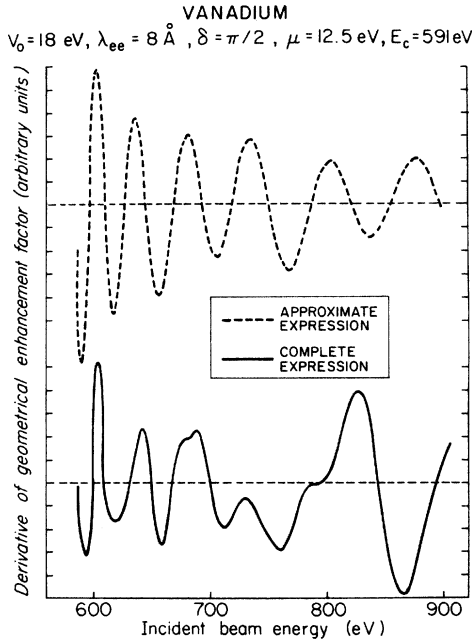

FIG. 2. Comparison between the full calculation of the derivative of the geometrical enhancement factor shown as the solid curve and the approximate expression of Eq. (2.43) shown as the dashed curve. The calculations are for a cluster of nine atoms having the geometry of bulk vanadium and use the other parameters shown in the figure.

and (2.28) and calculate G in the absence of initial-state scattering, i.e., by taking

$$A^-_{LL}(K(E_i), k_i) \rightarrow 0. \tag{3.4}$$

This is compared with the complete calculation in Fig. 3. Note that below ~715 eV there are only minor differences between the two curves but that at higher energies the differences become more significant. For our simple S-wave model, initial-state scattering effects are thus important for $E_i/\overline{E}_f \lesssim 5$. More realistic potentials will probably exhibit different values of the incident beam energy beyond which one must take proper account of initial-state scattering but the point is that there should be an energy beyond which initial-state scattering is important. Experimentally this will vary from system to system. Part (b) of Fig. 3 shows the same curves plotted as a function of the effective final-state momentum variable $\overline{k}_f$.

If a final-state scattering model is valid, then a simple Fourier transform given by

$$A(R) = \left| \int d(2\overline{k}_f) \exp(i2\overline{k}_f R)(dG/dE_i) \right| \tag{3.5}$$

should directly yield the shell spacing. In Fig. 4 we plot the absolute-value Fourier transform for the curves of Fig. 3 for two different ranges of the transform variable. In part (a) the transforms

VANADIUM

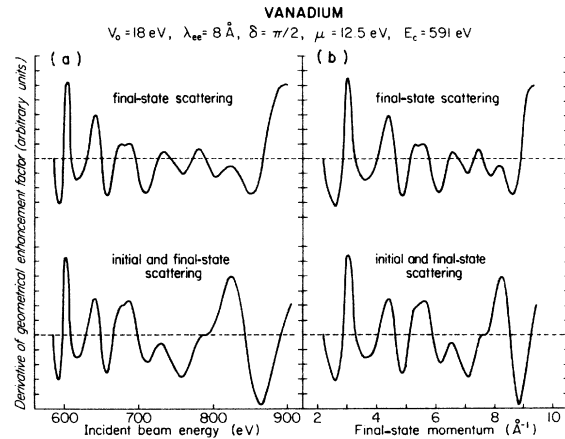$V_0 = 18 eV, \lambda_{ee} = 8 \text{ \AA}, \delta = \pi/2, \mu = 12.5 eV, E_c = 591 eV$

FIG. 3. Comparison of curves for the derivative of the geometrical enhancement factor calculated including both initial- and final-state scattering (lower curves) and only final-state scattering (upper curves). Part (a) shows the calculations as a function of the incident beam energy and part (b) shows the calculations as a function of the effective momentum variable $\overline{k}_f = [(2m/\hbar^2)(E_i + V_0 - \mu - \Delta)]^{1/2}$, where $\Delta = E_c - V_0$ is the binding energy of the core level relative to the muffin-tin zero. The calculations are for a cluster of nine atoms having the geometry of bulk vanadium and use the other parameters shown in the figure.
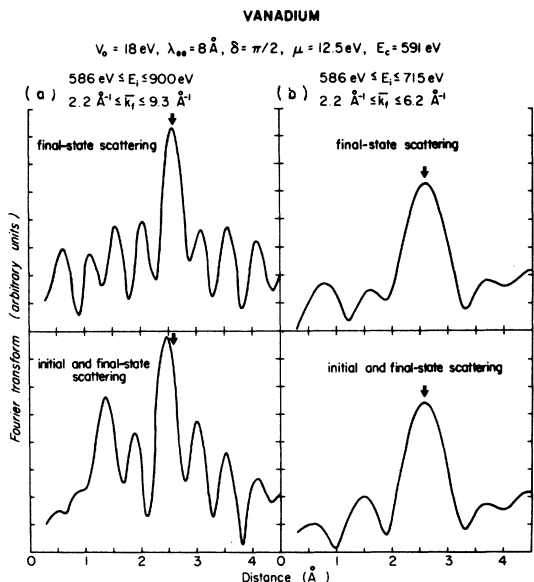
VANADIUM

$V_o = 18 eV,\ \lambda_{ee} = 8 \AA,\ \delta = \pi/2,\ \mu = 12.5 eV,\ E_c = 591\ eV$

(a) $586\ eV \leq E_i \leq 900\ eV$
     $2.2\ \AA^{-1} \leq \bar{k}_i \leq 9.3\ \AA^{-1}$

(b) $586\ eV \leq E_i \leq 715\ eV$
     $2.2\ \AA^{-1} \leq \bar{k}_i \leq 6.2\ \AA^{-1}$

final-state scattering

final-state scattering

initial and final-state scattering

initial and final-state scattering

FIG. 4. Comparison of absolute-value Fourier trans-
forms of the curves shown in Fig. 3. The curves in
part (a) are for the full range of the transform variable
and the curves in part (b) are for a restricted range of
the transform variable as indicated in the figure. The
calculations are for a cluster of nine atoms having the
geometry of bulk vanadium, and the arrows indicate the
position of the known shell spacing, which is 2.61 Å. The
other parameters used in the calculation are indicated
in the figure.

are taken over the full range $586 \leq E_i \leq 900$ eV
and in part (b) the transforms are taken only over
the range $586 \leq E_i \leq 715$ eV. The arrows indicate
the position of the "known" shell radius of 2.61 Å.
Since our model assumes constant phase shifts,
the only momentum dependence in the sine argu-
ments in Eq. (2.43) enters via the $2kR$ factor,
and we expect that the transforms should peak
exactly at $R = R_j$. In part (a) the transform of
the final-state-scattering calculation peaks exact-
ly at the correct position but the prominent peak
of the transform of the full calculation is off by
~0.1 Å. This latter accuracy is comparable with
LEED analysis but considerably poorer than that
of EXAFS. There are other prominent peaks in
the transform and for some model systems these
spurious peaks are so large as to make determina-
tion of the true signal difficult.[4] However, when
we restrict the range of our transform as in
part (b) these problems disappear. The main
signal peak is more clearly distinguishable from
the background and its position is within 0.02 Å
of the correct value. In real systems there are
additional momentum-dependent terms entering
the arguments of the sine functions. The deter-
mination of these provides an additional source

of error, but an analogous problem occurs in
EXAFS where a combination of model calcula-
tions[18,19] and a library of measured values is
used in data analysis. Analysis of APS extended
fine structure from transition-metal surfaces in-
dicates that reasonable estimates of the momen-
tum dependence of the central-atom phase shifts
and of the back-scatter phase factor can be ob-
tained from simple model potentials.[14] Restrict-
ing the transform range has the expected side
effect of broadening the signal peak and so for
any given system there will be some optimal
range over which to take the transform. However,
this approach may help to separate out the signal
from the noise. The transform peaks in our
model calculations are fairly narrow since only
one excitation-matrix element was included.
The contribution of several matrix elements in
the actual experiments makes the transform
peaks considerably broader.[14]

IV. EXTENDED FINE STRUCTURE IN CHARACTERISTIC LOSS MEASUREMENTS

A major potential complexity in interpreting the
APS extended fine structure lies in the fact that
there are no simple angular-momentum selec-
tion rules governing the electron-excited transi-
tions. In this section we consider the small-
momentum-transfer limit of the excitation process
and show that this yields the same dipole selection
rules as in photon-excited transitions. This ob-
servation is not unique to this work but has been
previously noted in connection with the interpre-
tation of EXAFS-like structure observed above
characteristic excitations in electron-energy-
loss measurements.[20-24] The purpose of this
section is to point out the connection between our
formalism and this body of work and also to give
an explicit expression for the oscillatory compo-
nent of the characteristic loss extended fine
structure. In doing this, we sketch out the neces-
sary approximations that yield the dipole selection
rules and give an estimate of the energy range
over which they are expected to be valid.

Although the general formalism of Sec. II is
applicable to the characteristic loss process in
all ranges of nonrelativistic energies and scat-
tering angles, the simplifications that occur in
certain regimes are more evident if we make
some initial approximations. First, we assume
that the energy of the incident electron is suffi-
ciently high that we can neglect any exchange
effects in the initial and final states. We also
neglect any scattering of the very-high-energy
initial- and final-state electrons (i.e., the mea-
sured electrons) from the lattice and so write

$$\langle \vec{r}_1, \vec{r}_2 \mid \psi_{\vec{k}_i}, \phi_c \rangle \simeq \chi_{\vec{k}_i}(\vec{r}_2)\phi_c(\vec{r}_1) \tag{4.1}$$

and

$$\langle \vec{r}_1, \vec{r}_2 \mid \psi_{\vec{k}_f}, \psi_{\vec{k}_{f'}} \rangle \simeq \chi_{\vec{k}_f}(\vec{r}_2)\psi_{\vec{k}_{f'}}(\vec{r}_1) . \tag{4.2}$$

Instead of making a partial-wave expansion of the interaction Hamiltonian, we write

$$H_1 = \frac{e^2}{|\vec{r}_1 - \vec{r}_2|} = 4\pi e^2 \int \frac{d^3q}{(2\pi)^3} \frac{\exp[i\vec{q}\cdot(\vec{r}_1 - \vec{r}_2)]}{q^2} . \tag{4.3}$$

The excitation-matrix element is then

$$M^c(\vec{k}_i; \vec{k}_f, \vec{k}_{f'}) \simeq 4\pi e^2 \int \frac{d^3r_1}{(2\pi)^3} \frac{\exp[i(\vec{k}_i - \vec{k}_f)\cdot\vec{r}_1]}{|\vec{k}_i - \vec{k}_f|^2}$$

$$\times \phi_c(\vec{r}_1)\psi^*_{\vec{k}_{f'}}(\vec{r}_1) . \tag{4.4}$$

We then assume that the momentum transfer is sufficiently small that we can make a power-series expansion of the exponential function over the region when $\phi_c(\vec{r}_1)$ is significant. For simplicity, we will let $\vec{k}_i - \vec{k}_f$ define the z axis of our system and make the usual partial-wave expansions of $\phi_c(\vec{r}_1)$ and $\psi^*_{\vec{k}_{f'}}(r_1)$. This yields

$$M^c(\vec{k}_i; \vec{k}_f, \vec{k}_{f'}) \simeq \frac{4\pi e^2}{|\vec{k}_i - \vec{k}_f|^2} \int \frac{d^3r_1}{(2\pi)^3} \sum_{LL'} [1 + i|\vec{k}_i - \vec{k}_f| r_1 \cos(\theta_1) + \cdots] R_{n_c l_c}(r_1) Y^*_{L_c}(\Omega_1)$$

$$\times \psi^{*L'}_{\vec{k}_{f'}L}(r_1) Y_{L'}(\Omega_1) Y_L(\Omega_{\vec{k}_{f'}})$$

$$= \frac{e^2 i}{2\pi^2 |\vec{k}_i - \vec{k}_f|} \sum_{LL'} I(L_c; L', \tfrac{1}{0}) \int_0^\infty dr_1 \, r_1^3 R_{n_c l_c}(r_1) \psi^{*L'}_{\vec{k}_{f'}L}(r_1) Y_L(\Omega_{\vec{k}_f}) . \tag{4.5}$$

$I(L_c; L', \tfrac{1}{0})$ is nonzero only for $l' = l_c \pm 1$ and $m_{l'} = m_c$, which gives us the familiar dipole selection rules. Using our previously derived expression for $\psi^{*L'}_{\vec{k}_{f'}L}(r_1)$, we obtain

$$M^c(\vec{k}_i; \vec{k}_f, \vec{k}_{f'}) = \sum_L [\exp(-i\delta'_l)\bar{B}^c_L(\vec{k}_i; \vec{k}_f, k_{f'}) + \exp(-i\delta'_l)\sum_{L'} \bar{B}^c_{L'}(\vec{k}_i; \vec{k}_f, k_{f'})A^*_{L'L}(K_{f'}, k_{f'})]Y_L(\Omega_{\vec{k}_f})$$

$$\equiv \sum_L M^c_L(\vec{k}_i; \vec{k}_f, k_{f'})Y_L(\Omega_{\vec{k}_f}) , \tag{4.6}$$

where

$$\bar{B}^c_L(\vec{k}_i; \vec{k}_f, k_{f'}) \equiv \frac{e^2 i}{2\pi^2 |\vec{k}_i - \vec{k}_f|} I(L_c; L, \tfrac{1}{0}) \times \int_0^\infty dr \, r^3 R_{n_c l_c}(r)\bar{\phi}^*_{k_{f'}}(r) . \tag{4.7}$$

The transition rate in a characteristic-loss measurement is given by

$$\dot{\mathcal{P}}_{\vec{k}_i \to \vec{k}_f} = \frac{2\pi N_c}{\hbar} \sum_{\vec{k}_{f'} > P_F} |M^c(\vec{k}_i; \vec{k}_f, \vec{k}_{f'})|^2 \delta(E_i - E_f - E_{f'} - \Delta)$$

$$= \frac{2\pi N_c}{\hbar} \rho(E_i - E_f - \Delta)\Theta(E_i - E_f - \Delta - \mu)\sum_L |M^c_L(\vec{k}_i; \vec{k}_f, \bar{k}_f)|^2 , \tag{4.8}$$

where now

$$\bar{k}_f = [(2m/\hbar^2)(E_i - E_f - \Delta)]^{1/2} . \tag{4.9}$$

and Θ is the Heaviside step function. Both E_i and E_f are measured outside the sample and now are referred to the vacuum level. We assume the same inner potential for both of these electrons.

Equation (4.9) takes a particularly simple form if the core level is an S state for then the only nonzero bare-excitation-matrix element is $\bar{B}^c_{(1,0)}$. The geometrical enhancement factor then becomes

$$G \simeq \frac{2\pi N_c}{\hbar} \rho(E_i - E_f - \Delta)\Theta(E_i - E_f - \Delta - \mu)|\bar{B}^{(0;0)}_{(1;0)}(\vec{k}_i; \vec{k}_f, \bar{k}_f)|^2$$

$$\times \left(2\,\text{Re}[A^*_{(1,0)(1,0)}(\bar{K}_f, \bar{k}_f)] + \sum_L A^*_{(1,0)L}(\bar{K}_f, \bar{k}_f)A_{(1,0)L}(\bar{K}_f, \bar{k}_f)\right) . \tag{4.10}$$

Evaluating G to first order in the lattice scattering and using the asymptotic expression of Eq. (2.38), we obtain for an S-state core level

$$G \simeq \frac{2\pi N_c}{\hbar} \rho(E_i - E_f - \Delta)\Theta(E_i - E_f - \Delta - \mu)|\bar{B}^{(0;0)}_{(1;0)}(\vec{k}_i; \vec{k}_f, \bar{k}_f)|^2 \sum_j F^{10,10}_j(\bar{k}_f, R_j) . \tag{4.11}$$

As in the case of EXAFS from an S-state core level,[8] one can divide by the background and eliminate the matrix element from the expression.

Based upon atomic calculations using the statistical-exchange approximation,[15] for vanadium the radius of the principle maximum in the $2S$ wave function lies at ~ 0.14 Å and the wave function itself is for practical purposes negligible beyond a radius of ~ 0.72 Å. Suppose we require for forward scattering in the expansion of Eq. (4.5)

$$|\vec{K}_i - \vec{K}_f| R_{\max} \lesssim \tfrac{1}{5}, \tag{4.12}$$

then we would want $|\vec{K}_i - \vec{K}_f| \lesssim 1.43$ Å^{-1} and would need an incident beam energy such that

$$\Delta = E_i - E_f \simeq (\hbar^2 k_i/m) |\vec{K}_i - \vec{K}_f|. \tag{4.13}$$

This would require $E_i \gtrsim 1.6 \times 10^5$ eV, which may be realizable in some electron microscopes. This estimate is very crude and it may not be necessary to go to these energies for actual data analysis as the relative sizes of the bare matrix elements are also important in determining which terms in the expansion dominate.

V. SUMMARY AND CONCLUSIONS

In summary, we have described how to incorporate the effects of the excited-central-atom potential into a calculation of the geometrically induced, extended fine structure above appearance potential thresholds. This involved treating the scattering from the central atom on a higher priority than scattering from the neighboring atoms and then expressing the remainder of the multiple-scattering problem in terms of the central-atom wave functions. Explicit expressions were given for the excitation-matrix elements. Following Lee and Pendry,[8] a series of approximations was made leading to an EXAFS-like result in that the dominant contribution to the APS extended fine structure could be written in terms of a series of sinusoidally varying functions. The end result is similar but not identical to that proposed in an earlier work[4] on the applicability of Fourier-transform techniques to APS data analysis. Unlike EXAFS, terms arise from both initial- and final-state scattering although there is a range where final-state scattering dominates. We then explored the major predictions of our model in the context of S-wave scattering from a cluster of sites having the atomic geometry of bulk vanadium and other parameters appropriate to the excitation of the $2S$ core state. It was shown that use of the renormalized basis set removes the overall phase shift between the single- and multiple-scattering limits noted in earlier calculations[3,4] using a plane-wave basis.

This was attributed to the phase renormalization introduced by the central-atom potential that was numerically included in the plane-wave-basis multiple-scattering calculations. We then compared the simplified approximate expression with the complete calculation and concluded that it adequately described the frequency of the oscillations but not their amplitude. This means that Fourier-transform techniques may yield the atomic shell radii but that it may be more difficult to determine the coordination numbers. We then explored the consequences of "turning off" the initial-state scattering and investigated the range of energies where final-state scattering dominates. If the Fourier transform is limited to this energy range, then the spurious peaks noted earlier[4] are much smaller. This argues that there is some optimal energy range for data analysis. Finally, we applied the formalism to extended fine structure that should occur above electron characteristic loss peaks and showed that in the small momentum transfer limit we return to the simple dipole selection rules of EXAFS. This may eliminate some of the complexities introduced by multiple angular-momentum final states in APS.

APPENDIX

In this appendix, we consider the solution to the integral equation defining $\phi_{\vec{K}}(\vec{r})$

$$\phi_{\vec{K}}(\vec{r}) = \chi_{\vec{K}}(\vec{r}) + \int d^3r_1 \, d^3r_2 \, G_0(\vec{r} - \vec{r}_1)$$
$$\times t_0(\vec{r}_1, \vec{r}_2) \chi_{\vec{K}}(\vec{r}_2). \tag{A1}$$

Utilizing the following Fourier transforms

$$G_0(\vec{r} - \vec{r}_1) = \int \frac{d^3k_1}{(2\pi)^3} \frac{\exp[i\vec{K}_1 \cdot (\vec{r} - \vec{r}_1)]}{E - (\hbar^2 k^2/2m) - \sum(E)} \tag{A2}$$

and

$$t_0(r_1, r_2) = \frac{\int d^3k_2 \, d^3k_3}{(2\pi)^6} \exp(i\vec{K}_2 \cdot \vec{r}_1 - i\vec{K}_3 \cdot \vec{r}_2)$$
$$\times t_0(\vec{K}_2, \vec{K}_3). \tag{A3}$$

Eq. (A1) becomes

$$\phi_{\vec{k}}(\vec{r}) = \chi_{\vec{k}}(\vec{r})$$

$$+ \int \frac{d^3 k_1}{(2\pi)^3} \frac{\chi_{\vec{k}_1}(\vec{r})}{E - (\hbar^2 k^2/2m) - \sum(E)} t_0(\vec{k}_1, \vec{k}) .$$

$$(A4)$$

Making the following partial-wave expansions

$$\phi_{\vec{k}}(\vec{r}) = \frac{1}{(2\pi)^{3/2}} \sum_L \phi_k^L(r) Y_L^*(\Omega_r) Y_L(\Omega_k) , \qquad (A5)$$

$$\exp(i\vec{k}\cdot\vec{r}) = \sum_L (4\pi)i^l j_l(kr) Y_L^*(\Omega_r) Y_L(\Omega_k) , \quad (A6)$$

and

$$t_0(\vec{k}_1, \vec{k}) = \sum_L t_0^{LL}(k_1, k) Y_L^*(\Omega_{k_1}) Y_L(\Omega_k) , \qquad (A7)$$

where j_l is the spherical Bessel function of order l, we obtain

$$\phi_k^L(r) = 4\pi(i)^l$$

$$\times \left(j_l(kr) + \int_0^\infty \frac{dk_1 k_1^2}{(2\pi)^3} \frac{j_l(k_1 r) t_0^{LL}(k_1, k)}{E - (\hbar^2 k^2/2m) - \sum(E)} \right) .$$

$$(A8)$$

It is simple to evaluate Eq. (A8) in the large-r limit (i.e., outside the muffin-tin radius) yielding

$$\phi_k(r > R_{m_t}) = 4\pi(i)^l$$

$$\times \left(j_l(kr) - \frac{m\pi K i}{\hbar^2} \frac{h_l^{(1)}(Kr)}{(2\pi)^{3/2}} t_0^{LL}(K, k) \right) ,$$

$$(A9)$$

where

$$\hbar^2 K^2/2m = E - \sum(E) , \qquad (A10)$$

and $h_l^{(1)}$ is the spherical Hankel function of the first type. We only require solutions on the complex energy shell—i.e., for $k = K$—and hence can take

$$t_0^{LL}(K, K) = \frac{4\pi^2 i \hbar^2}{mK} [\exp(2i\delta_l) - 1] , \qquad (A11)$$

where δ_l is the usual energy-dependent partial-

wave phase shift for the central-atom potential. With some algebraic manipulation, Eq. (A9) can be rewritten as

$$\phi_K(r > R_{m_t}) = 2\pi(i)^l \exp(i\delta_l)$$

$$\times [\exp(i\delta_l) h_l^{(1)}(Kr)$$

$$+ \exp(-i\delta_l) h_l^{(2)}(Kr)] , \qquad (A12)$$

which is the usual sum of an ingoing and an outgoing wave *apart* from the $\exp(i\delta_l)$ prefactor. Hence, in order to match to this wave function at the muffin-tin radius, the interior solutions must have the form

$$\phi_k(\vec{r} < R_{m_t}) = \sum_L Y_L^*(\Omega_r) \overline{\phi}_k^l(r) \exp(i\delta_l) , \qquad (A13)$$

where $\overline{\phi}_k^l(r)$ is the usual numerical solution to the radial-wave-function equation

$$-\frac{1}{r^2} \frac{d}{dr} \frac{[r^2 d\overline{\phi}_k^l(r)]}{dr}$$

$$+ \left(\frac{l(l+1)}{r^2} + V(r) \right) \overline{\phi}_k^l(r) = E\overline{\phi}_k^l(r) . \quad (A14)$$

This overall phase factor has been noted by Liebsch[25] in his work on photoemission from localized core levels but does not appear explicitly in the theoretical description of EXAFS put forth by Lee and Pendry.[8] However, since the calculation of physical quantities involves the magnitude squared of matrix elements, this choice of phase is somewhat arbitrary. We use the definitions of $\phi_k(r)$ given by Eqs. (A12) and (A13) and obtain an expression analogous to that of Lee and Pendry,[8] although the various contributions to the "phase" of the sinusoidally varying functions enter in different ways. Following the approach used in LEED calculations, we calculate phase shifts and evaluate Eq. (A14) ignoring the imaginary part of the complex optical potential defined by $\sum(E)$. This means that we calculate $\overline{\phi}_k^l(r)$ in Eq. (A14) for

$$\hbar^2 k^2/2m = E \qquad (A15)$$

and analytically continue $k \to K$ as needed.

[1] P. I. Cohen, T. L. Einstein, W. T. Elam, Y. Jukuda, and R. L. Park, Appl. Suf. Sci. 1, 538 (1978).

[2] W. T. Elam, P. I. Cohen, L. Roelofs, and R. L. Park, Appl. Surf. Sci. 2, 636 (1979).

[3] G. E. Laramore, Phys. Rev. B 18, 5254 (1978).

[4] G. E. Laramore, Surf. Sci. 81, 43 (1979)

[5] D. E. Sayers, E. A. Stern, and F. W. Lytle, Phys. Rev.

Lett. 27, 1204 (1971).

[6] D. E. Sayers, F. W. Lytle, and E. A. Stern, in *Advances in X-ray Analysis*, edited by B. L. Henke, J. B. Newkirk, and G. R. Mallet (Plenum, New York, 1970).

[7] M. L. den Boer, T. L. Einstein, W. T. Elam, R. L. Park, L. D. Roelofs, and G. E. Laramore, J. Vac. Sci. Technol. (to be published).

[8]P. A. Lee and J. B. Pendry, Phys. Rev. B **11**, 2795 (1975).

[9]There are many ways of parametrizing the one-electron LEED wave functions. We use the approach originally developed by Duke and Tucker, e.g., C. B. Duke and C. W. Tucker, Jr., Phys. Rev. Lett. **23**, 1163 (1969); Surf. Sci. 15, 231 (1969).

[10]See, for example, M. L. Goldberger, and K. M. Watson, *Collision Theory* (Wiley, New York, 1965), Chap. 2.

[11]See, for example, C. B. Duke and G. E. Laramore, Phys. Rev. B **2**, 4765 (1970).

[12]T. L. Einstein, L. D. Roelofs, R. L. Park, and G. E. Laramore, Bull. Am. Phys. Soc. **24**, 506 (1979).

[13]For simplicity, we will ignore the effects of the lattice vibrations. These could be included in an approximate way by renormalizing the single-site t matrix as done in LEED calculations.

[14]W. T. Elam, P. I. Cohen, L. D. Roelofs, and R. L. Park, Bull. Am. Phys. Soc. **24**, 506 (1979).

[15]D. Liberman, J. T. Waber, and D. T. Cromer, Phys. Rev. A **27**, 137 (1965).

[16]K. Siegbahn, C. Nordling, A. Fahlman, R. Nordbeny,

K. Hamrin, J. Hedman, G. Johansson, T. Boegwark, S. Karlsoon, I. Lindgren, and B. Lindberg, *ESCA: Atomic, Molecular and Solid State Structure Studied by Means of Electron Spectroscopy* (Almqvist and Wiksells, Uppsala, 1967), Appendix I.

[17]G. E. Laramore, Phys. Rev. B **8**, 515 (1973).

[18]B. K. Teo, P. A. Lee, A. L. Simons, P. Eisenberger, and B. M. Kincaid, J. Am. Chem. Soc. **99**, 3854 (1977).

[19]P. A. Lee, B. K. Teo, and A. L. Simons, J. Am. Chem. Soc. **99**, 3856 (1977).

[20]C. Colliex and B. Jouffrey, Philos. Mag. **25**, 491 (1972).

[21]J. J. Ritsko, S. E. Schnatterly, and P. C. Gibbons, Phys. Rev. Lett. **32**, 671 (1974).

[22]R. D. Leapman and V. E. Cosslett, J. Phys. D **9**, 229 (1976).

[23]B. M. Kincaid, A. E. Meixner and P. M. Platzman, Phys. Rev. Lett. **40**, 1296 (1978).

[24]P. E. Batson and A. J. Craven, Phys. Rev. Lett. **42**, 893 (1979).

[25]A. Liebsch, Phys. Rev. B **13**, 544 (1976).